Global Journal of Pure and Applied Mathematics.
ISSN 0973-1768 Volume 15, Number 5 (2019), pp. 637-648

http://www.ripublication.com/gjpam.htm

Analysis of the Effect of Stretching Parameter and Time Parameter on MHD Nanofluid Flow in the Presence of Suction

[1]Virginia M. Kitetu, [2]Thomas T. M. Onyango, [3]Jackson K. Kwanza

[1]Department of Mathematics and Actuarial Science, Catholic University of Eastern Africa, Box 62157-00200, Nairobi- Kenya.

[2]Department of Industrial and Engineering Mathematics, Technical University of Kenya, Box 52428-00200, Nairobi- Kenya.

[3]Department of Pure and Applied mathematics, Jomo Kenyatta University of Agriculture and Technology, Box 62000-00200, Nairobi- Kenya.

Abstract

In this paper a two dimensional MHD boundary layer nanofluid flow as a result of stretching surface is explored. Nanofluid play an important role in heat transfer systems and hence the researchers have used copper-water and silver-water nanofluid in this study. Similarity transformation is used to non-dimensionalize momentum, temperature and concentration equations which describe this flow physically. The reduced coupled partial differential equations (PDEs) are linearized using finite volume method (FVM). The impact of stretching parameter and time parameter on velocity, temperature, concentration, skin friction, Nusselt and Sherwood number is studied then results are illustrated graphically. It is observed that stretching parameter increase velocity of nanofluid. In addition, increase in time parameter results to increase in temperature and concentration.

Keywords: Hartmann number, time parameter, nanofluid, MHD, suction.

1. INTRODUCTION

Nanoparticles can be suspended in industrial heat transfer fluids such as water, ethylene glycol, or oil to enhance heat transfer because their thermal conductivity is higher compared to the fluids. Because of high rate of heat transfer nanofluid is used by engineers for cooling purposes in polymer extraction, drawing of wires, manufacturing of plastic sheets, and production of glass frames, drawing, heating, cooling and thinning of copper wire. Nanofluid being a fluid of substance, researchers have conducted

studies on nanofluid flow on stretching surface: Unsteady MHD free convection flow past a vertical permeable flat plate in a rotating frame of reference with constant heat source in a nanofluid was discussed by [3]. They considered nanofluid flow past an oscillatory moving vertical permeable semi-infinite flat plate with constant heat source. The velocity along the plate, which is also known slip velocity was assumed to oscillate on time with a constant frequency. The analytical solutions of the boundary layer equations were assumed of oscillatory type and they were obtained by using the small perturbation approximations. The influence of various relevant physical characteristics were presented and discussed. Boundary layer flow past a stretching/shrinking surface beneath an external uniform shear flow with a convective surface boundary condition in a nanofluid was explored by [8]. Governing PDEs were changed to ODEs using a similarity transformation. The ODEs were solved using Runge-Kutta-Fehlberg method with shooting technique. Copper-water and silver-water nanofluid were used and impact of nanoparticle volume fraction, the type of nanoparticles, the convective parameter, and the thermal conductivity on the heat transfer characteristics were evaluated. Results showed that, heat transfer rate at the surface increased when nanoparticle volume fraction was increased and decreased with the convective parameter. Rate of heat transfer at the surface of copper-water nanofluid was higher compared to the one of surface of silver-water nanofluid although thermal conductivity of silver is higher than that of copper. [9], explored finite element simulation of unsteady magneto-hydrodynamic transport phenomena on a stretching sheet in a rotating nanofluid. They focused on boundary layer flow and heat transfer in an incompressible rotating nanofluid over a stretching continuous sheet and transverse magnetic field applied normal to the sheet plane. Continuity, momentum, energy and concentration equation were normalized into a system of two-dimensionless boundary layer equations through scaling transformations. Finite element method (FEM) based on the variation formulation was used to solve the nonlinear two-point boundary value problem. FEM was found to be a robust and efficient. Impacts of the physical parameters on the velocity components, temperature and nanoparticle concentration was illustrated graphically. Velocity retarded with increased Hartmann number but temperature and nanoparticle concentration were increased by the Hartmann number. Velocity, temperature and nanoparticle concentration were decreased by increased rotational. A recent research on stagnation point flow of a nanofluid toward an exponentially stretching sheet with non-uniform heat generation was examined by [6]. The model they used was composed of two component and non-homogeneous equations that incorporated the effects of Brownian diffusion and thermophoresis. PDEs boundary layer equations were reduced to a two-point boundary value problem through similarity variables and solved analytically. Effects of heat generation, stretching parameter, thermophoresis, Lewis number, Brownian motion and Prandtl number on heat transfer and concentration rates were investigated. From the results, heat transfer and concentration rates increased when stretching parameter was increased. Discussion of transient magnetohydrodynamic radiative free convection nanofluid flow from a stretching permeable surface was examined by [2]. They concentrated on mixed convective laminar boundary layer flow of an incompressible, viscous, dissipative, electrically conducting nanofluid from a continuously stretching

permeable surface in the presence of magnetic field and thermal radiation flux. Time dependent stretching velocity and surface temperature and concentration represented unsteadiness in the momentum, temperature, and concentration fields. Similarity transformations converted the governing time-dependent nonlinear boundary layer equations to a system of nonlinear coupled ODEs together with boundary conditions. Magnetic parameter, thermal convective parameter, mass convective parameter, suction parameter, radiation-conduction parameter, Eckert number, Prandtl number, Lewis number, Brownian motion parameter, thermophoresis parameter, and the unsteadiness parameter effect to flow was examined. Robust Nactsheim Swigert shooting method and sixth order Runge-Kutta iterative method were used to obtain numerical solution. Their solution were in agreement with previously published work. [1], studied MHD boundary layer flow and heat transfer characteristics of a nanofluid over a stretching surface sheet. Radiative heat transfer in a nanofluid influenced by magnetic field over a stretching surface was researched. PDEs which governed the flow were converted into nonlinear ODEs through using similarity transformation. Numerical scheme known as Nactsheim-Swigert shooting technique and Runge-Kutta six order iteration method was used to solve the ODEs. Numerical solution excellently agreed with published work. An investigation on significance of Darcy Forchheimer porous medium in nanofluid nanotubes was conducted by [5]. They considered bidirectional nonlinear surface which was stretchable. They used Darcy forchheimer expression which helped them study convective heat mechanism. Optimal homotopic solutions for velocity and temperature were shown graphically. A recent study on model for MHD viscoelastic nanofluid flow with prominence effects of radiation was researched by [4]. They explored steady state flow of an incompressible viscoelastic nanofluid through a permeable plate. The impact of viscoelastic, magnetic, radiation and nanofluid parameter was analyzed. Graphs for velocity, temperature, concentration were drawn.

2. DESCRIPTION AND FORMULATION

2.1 Description of problem

Consider unsteady laminar MHD mixed convective nanofluid flow as a result of straight porous stretching surface situated at x axis with stretching velocity $u = bx$, where b is a constant: For stretching surface $b > 0$ and for a shrinking surface $b < 0$. Let suction velocity be $v = v_w$ the temperature at the wall is $T = T_w$ and nanoparticle concentration at the stretching surface is $C = C_w$. The temperature of the free stream nanofluid is $T = T_\infty$ and and the ambient concentration is C_∞. The x is along the stretching surface and y direction is orthogonal to the stretching surface. The flow experiences magnetic force.

The initial and boundary conditions are respectively:

$u = 0, v = 0, T = T_w, C = C_w \; at \; t < 0,$

$u = U_w = bx,\ \ v = v_w,\ \ T = T_w,\ \ C = C_w : y = 0, t \geq 0$
$u = U_\infty = b_\infty x,\ \ v = 0,\ \ T = T_\infty,\ \ C = C_\infty : y \to \infty, t \geq 0'$

where $v_w < 0$ is suction velocity while $v_w > 0$ is blowing velocity and b_∞ denotes stagnation flow rate parameter.

The properties of nanofluid are defined as follows, Haroun *et al* (2015)

$$\mu_{nf} = \frac{\mu_f}{(1-\Phi)^{2.5}}, k_{nf} = k_f\left(\frac{k_s + k_f + 2\Phi(k_s - k_f)}{k_s + 2k_f + \Phi(k_s - k_f)}\right), (\rho c_p)_{nf}$$
$$= (1-\Phi)(\rho c_p)_f + \Phi(\rho c_p)_s, \rho_{nf} = (1-\Phi)\rho_f + \Phi\rho_s, \Phi_0$$
$$= (1-\Phi)^{2.5}\left(1 - \Phi + \Phi\left(\frac{\rho_s}{\rho_f}\right)\right), \Phi_a = \left(1 - \Phi + \Phi\frac{(\rho c_p)_s}{(\rho c_p)_f}\right)$$

where the subscripts f denote base fluid while s represent the nanoparticle. In this study Φ represent nanoparticle volume fraction. The thermal properties of base fluid and nanoparticle are in the table below.

Table 1: Thermal physical properties of pure water, copper and silver nanoparticles

Physical properties	Base fluid (water)	Copper	Silver (Ag)
c_p(j/kgk)	4179	385	235
$\rho(kg/m^3)$	997.1	8933	10500
$k(w/mk)$	0.613	401	429
$\alpha \times 10^7(m^2/s)$	1.47	1163.1	1738.6
$\beta \times 10^5(k^{-1})$	21	1.67	1.89

2.2 Governing equations

The nanofluid flow is governed by continuity, momentum, thermal energy and concentration boundary layer equations:

$$\frac{\partial u}{\partial x} + \frac{\partial v}{\partial y} = 0. \quad (1)$$

$$\frac{\partial u}{\partial t} + u\frac{\partial u}{\partial x} + v\frac{\partial u}{\partial y} = -\frac{1}{\rho_{nf}}\frac{\partial p}{\partial x} + \vartheta_{nf}\frac{\partial^2 u}{\partial y^2} + g_a B_T(T - T_\infty) + g_a B_C(C - C_\infty) - \sigma {B_0}^2 u. \quad (2)$$

$$\frac{\partial T}{\partial t} + u\frac{\partial T}{\partial x} + v\frac{\partial T}{\partial y} = \alpha_{nf}\frac{\partial^2 T}{\partial y^2} + \frac{\rho_f D_m k_T}{C_s \rho_{nf}(c_p)_{nf}}\frac{\partial^2 C}{\partial y^2} + \frac{Q}{\rho_{nf}(c_p)_{nf}}(T - T_\infty). \quad (3)$$

$$\frac{\partial C}{\partial t} + u\frac{\partial C}{\partial x} + v\frac{\partial C}{\partial y} = D_m\frac{\partial^2 C}{\partial y^2} + \frac{D_m k_m}{T_m}\frac{\partial^2 T}{\partial y^2} - R(C - C_\infty), \quad (4)$$

where u, v, T and C denote velocity component along x axis, velocity component along y axis, temperature and concentration respectively. In the free stream momentum equation (2) reduces to

$$\frac{1}{\rho_{nf}}\frac{\partial p}{\partial x} = -U_\infty \frac{dU_\infty}{dx} - \sigma \frac{B_0^2}{\rho_{nf}} U_\infty \,. \tag{5}$$

Substituting equation (5) into equation (2) momentum equation simplifies to:

$$\frac{\partial u}{\partial t} + u\frac{\partial u}{\partial x} + v\frac{\partial u}{\partial y} = \vartheta_{nf}\frac{\partial^2 u}{\partial y^2} + U_\infty \frac{dU_\infty}{dx} + (U_\infty - u)\sigma \frac{B_0^2}{\rho_{nf}} + g\beta_T(T - T_\infty) + g_a\beta_C(C - C_\infty). \tag{6}$$

In order to satisfy continuity equation a stream function, Haroun *et al* (2015):

$$\varphi = \sqrt{b_\infty \vartheta_f \varepsilon} x f(\varepsilon, n), \tag{7}$$

is introduced and

$$u = \frac{\partial \varphi}{\partial y}, v = -\frac{\partial \varphi}{\partial x}. \tag{8}$$

3. NON-DIMENSIONALIZING GOVERNING EQUATIONS

Equations (1), (3), (4) and 6) are non-dimensionalized using dimensionless variables; namely dimensionless length along y direction n, dimensionless time ε, dimensionless stream function $f(\varepsilon, n)$, dimensionless temperature $\theta(\varepsilon, n)$ and dimensionless concentration $\emptyset(\varepsilon, n)$

$$y = n\sqrt{\frac{\vartheta_f \varepsilon}{b_\infty}},\ \ \varepsilon = 1 - e^{b_\infty t},\ \ f(\varepsilon, n) = \frac{1}{\sqrt{a_\infty \vartheta_f \varepsilon x}},\ \ \frac{\theta(n)}{g(\varepsilon)} = \frac{T - T_\infty}{T_w - T_\infty}$$
$$\frac{\emptyset(n)}{g(\varepsilon)} = \frac{C - C_\infty}{C_w - C_\infty} \tag{9}$$

Using equations (7), (8) and (9) the governing equations (3), (4) and (6) reduces to:

$$f''' + \Phi_0\left[(1-\varepsilon)\frac{n}{2}f'' + \varepsilon\left(-f'^2 + ff'' + 1 + Ha^2(1 - f') + Gr_T\frac{\theta}{g(\varepsilon)} + Gr_C\frac{\emptyset}{g(\varepsilon)}\right)\right] = \Phi_0\varepsilon(1-\varepsilon)\frac{\partial}{\partial\varepsilon}f' \tag{10}$$

$$\theta'' + \frac{k_f}{k_{nf}}pr\Phi_a\left\{\frac{n}{2}(1-\varepsilon)\theta' + \varepsilon[f\theta' + \sigma\theta] + \frac{D_f}{\Phi_a}\emptyset''\right\} = -\frac{k_f}{k_{nf}}pr\Phi_a\varepsilon(1-\varepsilon)\frac{\theta g_\varepsilon}{g}. \tag{11}$$

$$\emptyset'' + Sc\left[\frac{n}{2}(1-\varepsilon)\emptyset' + \varepsilon(f\emptyset' - \gamma\emptyset) + Sr\theta''\right] = -Sc\varepsilon(1-\varepsilon)\frac{\emptyset}{g}g_\varepsilon. \tag{12}$$

where $g_\varepsilon = \frac{\partial g}{\partial \varepsilon} = q$, then $g = \varepsilon q$ and q is a constant. (13)

The non-dimensionalized boundary conditions and initial conditions are respectively:

$$f(\varepsilon, 0) = f_w, f'(\varepsilon, 0) = \lambda, \theta(\varepsilon, 0) = \varepsilon, \emptyset(\varepsilon, 0) = \varepsilon\ at\ n = 0, \varepsilon \geq 0 \tag{14}$$

$$f'(\varepsilon, \infty) = 1, \theta(\varepsilon, \infty) = 0, \emptyset(\varepsilon, \infty) = 0, as\ n \to \infty, \varepsilon \geq 0 \tag{15}$$

Using equation (13) and considering the case where, $\varepsilon = 1$, $t \to \infty$, corresponding to $f(n, 1) \approx f(n), \theta(n, 1) \approx \theta(n)\ and\ \emptyset(n, 1) \approx \emptyset(n)$. In this case equations (10), (11) and (12) reduce to:

$$\frac{d^3f}{dn^3} + \Phi_0\left[f\frac{d^2f}{dn^2} - \left[\frac{df}{dn}\right]^2 + 1 + Ha^2\left(1 - \frac{df}{dn}\right) + Gr_T\theta + Gr_C\emptyset\right] = 0. \quad (16)$$

$$\frac{d^2\theta}{dn^2} + \frac{k_f}{k_{nf}}Pr\Phi_a\left(f\frac{d\theta}{dn} + \delta_a\theta\right) + \frac{k_f}{k_{nf}}PrD_f\frac{d^2\emptyset}{dn^2} = 0. \quad (17)$$

$$\frac{d^2\emptyset}{dn^2} + Sc\left(f\frac{d\emptyset}{dn} - \gamma\emptyset\right) + ScSr\frac{d^2\theta}{dn^2} = 0. \quad (18)$$

From the non-dimensionalizing the following dimensionless parameters are obtained:

$$Pr = \frac{\vartheta_{nf}}{\alpha_{nf}}, Gr_T = \frac{g\beta_T(T_w - T_\infty)}{b_\infty^2 x}, Gr_c = \frac{D_m K_T(C_w - C_\infty)}{b_\infty^2 x}, Ha^2 = \frac{\sigma {B_0}^2}{b_\infty \rho_{nf}}, \delta_a = \frac{Q}{b_\infty(\rho c_p)_{nf}}, D_f = \frac{D_m k_T(C_w - C_\infty)}{C_s(c_p)_f \vartheta_f(T_w - T_\infty)}, sc = \frac{\vartheta_{nf}}{D_m}, \gamma = \frac{R}{b_\infty}, sr = \frac{D_m k_T(T_w - T_\infty)}{T_m \vartheta_f(C_w - C_\infty)}$$

Equations (16), (17) and (18) are discretized using FVM to obtain equations:

$$\frac{1}{\Delta n}f'_{i-1} - \left(\frac{2}{\Delta n} + Ha^2\Delta n\right)f'_i + \frac{1}{\Delta n}f'_{i+1} = -\Phi_0\left\{\frac{f_i}{2}\left(f'_{i+1} - f'_{i-1}\right) - \left(f'_i\right)^2\Delta n + \Delta n + Ha^2\Delta n + Gr_T\theta_i\Delta n + Gr_C\emptyset_i\Delta n\right\}, \quad (19)$$

$$\frac{1}{\Delta n}\theta_{i-1} + \left(\frac{-2}{\Delta n} + \frac{k_f}{k_{nf}}pr\Phi_a\delta_a\Delta n\right)\theta_i + \frac{1}{\Delta n}\theta_{i+1} = -\frac{k_f}{2k_{nf}}pr\Phi_a f'_i(\theta_{i+1} - \theta_{i-1}) - \frac{k_f}{k_{nf}}prD_f\left(\frac{\emptyset_{i+1}}{\Delta n} - \frac{2\emptyset_i}{\Delta n} + \frac{\emptyset_{i-1}}{\Delta n}\right) \quad (20)$$

$$\frac{1}{\Delta n}\emptyset_{i-1} - \left(\frac{2}{\Delta n} + Sc\gamma\Delta n\right)\emptyset_i + \frac{1}{\Delta n}\emptyset_{i+1} = -\frac{Scf_i}{2}(\emptyset_{i+1} - \emptyset_{i-1}) - ScSr\left(\frac{\theta_{i+1}}{\Delta n} - \frac{2\theta_i}{\Delta n} + \frac{\theta_{i-1}}{\Delta n}\right). \quad (21)$$

Skin friction, Nusselt number and Sherwood numbers are given by equations (22), (23) and (24) respectively:

$$C_f = -\frac{2}{\rho_f {U_\infty}^2}\frac{U_\infty\mu_f}{(1-\Phi)^{2.5}x}\sqrt{\frac{U_\infty x}{\vartheta_f\varepsilon}}f_{nn}(0,\varepsilon) = -\frac{2}{\sqrt{(1-\Phi)^5}}\frac{f_{nn}(0,\varepsilon)}{\sqrt{\varepsilon Re}}, \quad (22)$$

$$Nu = -\frac{k_{nf}}{k_f}\sqrt{\frac{Re}{\varepsilon}}\theta_n(0,\varepsilon), \quad (23)$$

$$Sh = -\left(\frac{Re_x x}{\varepsilon}\right)^{\frac{1}{2}}\emptyset_n(0,\varepsilon). \quad (24)$$

4. RESULTS AND DISCUSSION

To understand the flow problem physically results for equations (19) to (21) are presented graphically for variation of stretching and time parameter.

Graphs in figure 1 to figure 3, are drawn using table 1 and $\Phi = 0.2,\ f_w = 1, Df = 0.01, \lambda = -2, 0, 2,\ Gr_T = 0.01, Gr_C = 0.01, Pr = 7, sc = 1, sr = 1, \delta_a = 0.2, Ha = 2, \gamma = 3,\ \varepsilon = 0.3, 0.6, 0.9$ and $Re = 1$. Graphs in figure 4 to figure 6 are obtained using table 1 and $\Phi = 0.2,\ f_w = 1, Df = 0.01, \lambda = 2, Gr_T = 0.01, Gr_C = 0.01, Pr = 7, sc = 1, sr = 1, \delta_a = 0.1, Ha = 2, \gamma = 3,\ \varepsilon = 1$ and $Re = 1$

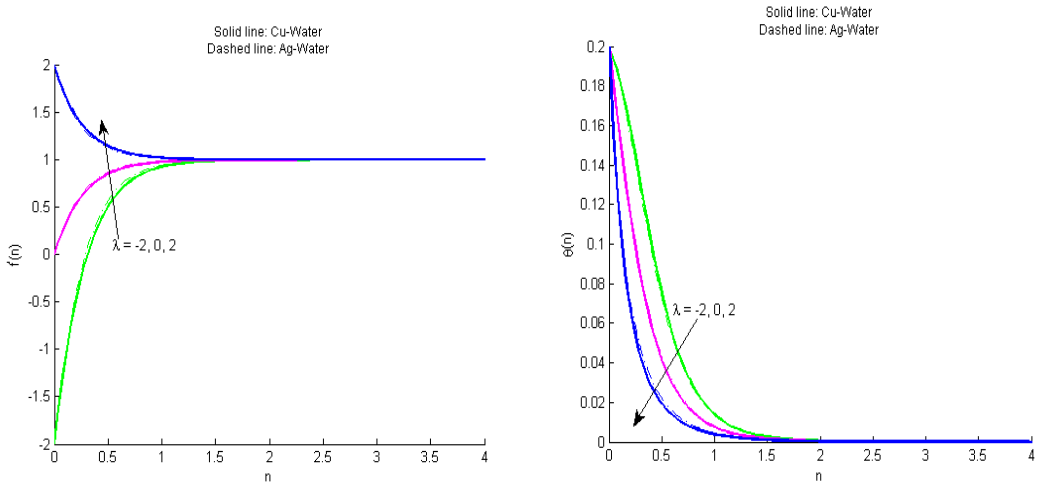

(a) (b)

Figure 1: (a) Velocity and (b) concentration profiles when varying stretching parameter

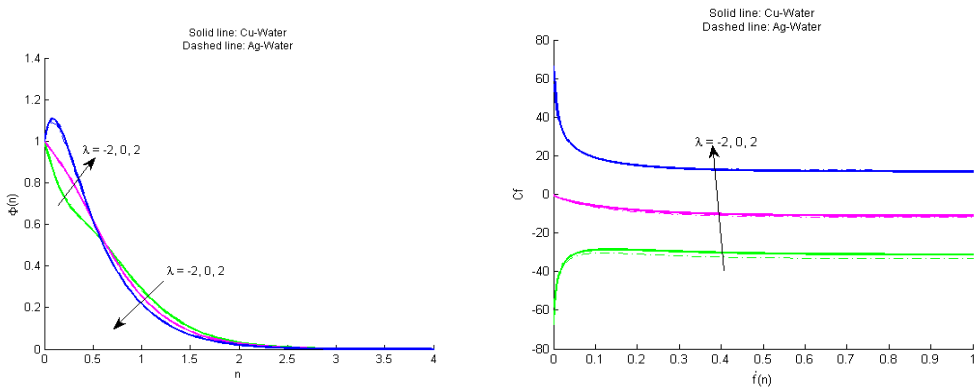

(a) (b)

Figure 2: (a) Velocity and (b) concentration profiles when varying stretching parameter

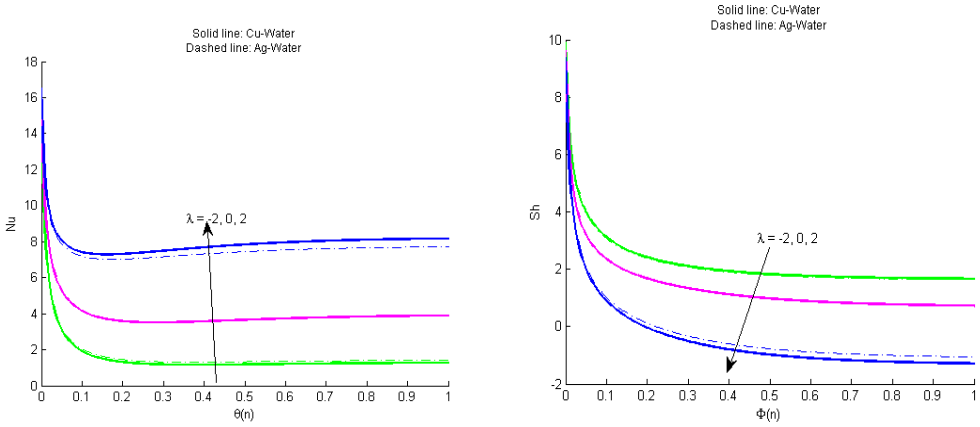

(a) (b)

Figure 3: (a) Heat transfer and (b) mass transfer coefficients when varying stretching parameter

In figure 1(a) increase in stretching parameter ($\lambda = 2$) increases velocity of nanofluid. This is caused by stretch which reduce viscous effect on the flow. As a result momentum boundary layer thickness is reduced with increasing stretching parameter hence increased nanofluid velocity. For a shrinking surface ($\lambda = -2$) velocity of nanofluid decreases when the shrinking parameter is increased. This is because of resistance to movement of the flow due high viscosity hence velocity is not enhanced. This makes the thickness of the velocity boundary layer to increase hence decreased velocity. Velocity of both nanofluid increases with increasing n for shrinking surface. As observed from figure 1(b), the temperature reduces when the stretching parameter is increased because stretching enhances nanofluid velocity which in turn increases thermal boundary layer thickness hence high temperature gradients on the surface. The thermal boundary layer thickness for silver-water nanofluid is smaller compared to the one of copper-water nanofluid. This caused by higher thermal conductivity of silver than copper and consequently, silver-water nanofluid temperature is higher compared to the one of copper-water nanofluid. Observation from figure 1(c) is that, on the surface concentration increase with increasing value of stretching parameter up to a critical value of n. Beyond the critical point, the concentration decreases with increase of stretching parameter. This is because on the surface the nanofluid velocity is enhanced hence increased concentration while beyond the critical point effect of stretching surface on velocity are not felt resulting to decreased concentration . Skin friction coefficient increase when the stretching parameter is increased implying that the shear stress is more at the stretching surface as seen in figure 2(a). Silver-water nanofluid has more skin friction when compared to copper-water nanofluid since silver-water nanofluid has lower velocity than copper-water nanofluid velocity hence increased surface drag for the case of silver-water nanofluid. When the shrinking parameter increases $\lambda = -2$, the skin friction coefficient decreases implying that shear stress is less at the shrinking surface. Skin friction coefficient for silver-water nanofluid is lower than the one for copper-water nanofluid, see figure (2b) for a shrinking surface. It is

observed that from figure 3(a), heat transfer coefficient increases when stretching parameter is increased but mass transfer decrease with increasing value of the shrinking parameter. From figure 3(b) rate of mass transfer decrease with increase of stretching parameter on the stretching surface but increase with increasing shrinking parameter. This caused by decreased surface drag for shrinking surface. Silver-water nanofluid has higher Sherwood number than copper-water nanofluid because it less viscous.

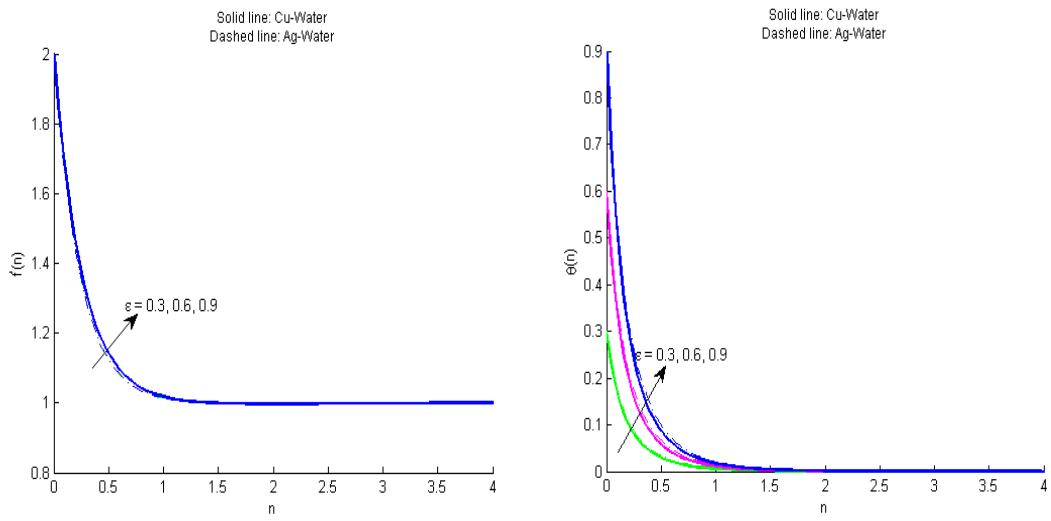

(a) (b)

Figure 4: (a) Velocity and (b) temperature profiles when varying dimensionless time parameter

From figure 4(a) the velocity of nanofluid remains constant when dimensionless time parameter is increased. This means that dimensionless time does not significantly affect the nanofluid velocity. Silver-water nanofluid has less velocity than copper-water nanofluid because it has higher viscosity. When dimensionless time parameter is increased, temperature also increases, figure 4(b). Silver-water nanofluid have higher temperature compared to copper-water nanofluid, figure 4(b). This is because copper has lower thermal conductivity than silver. Using figure 5(a), when dimensionless time parameter is increased concentration also increases. At the surface concentration increase for each value of ε then decrease as the flow regime develops. This is caused by mass diffusion within the concentration boundary layer region. Temperature decrease with increasing value of n high molecular diffusion on the surface.

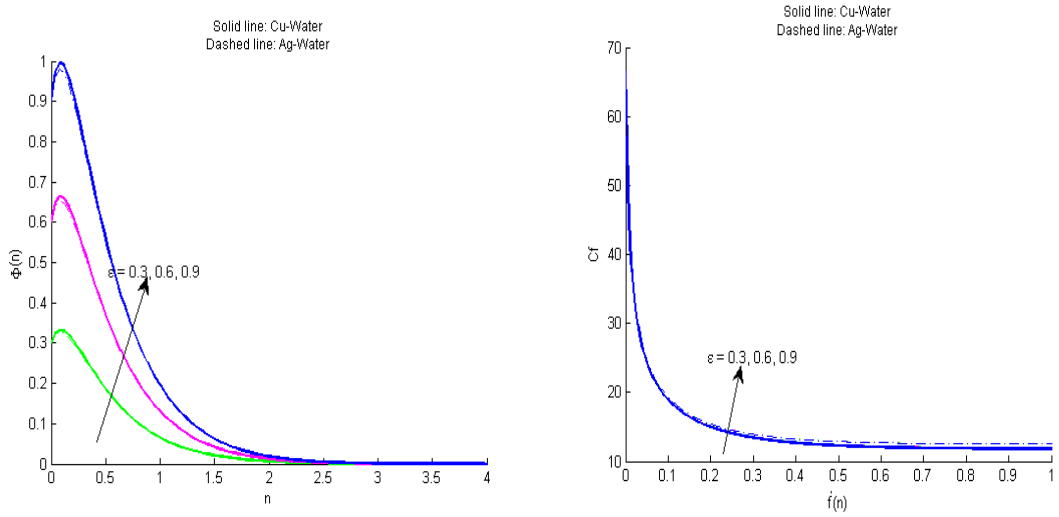

(a) (b)

Figure 5: (a) Concentration profiles and heat transfer coefficient when varying dimensionless time

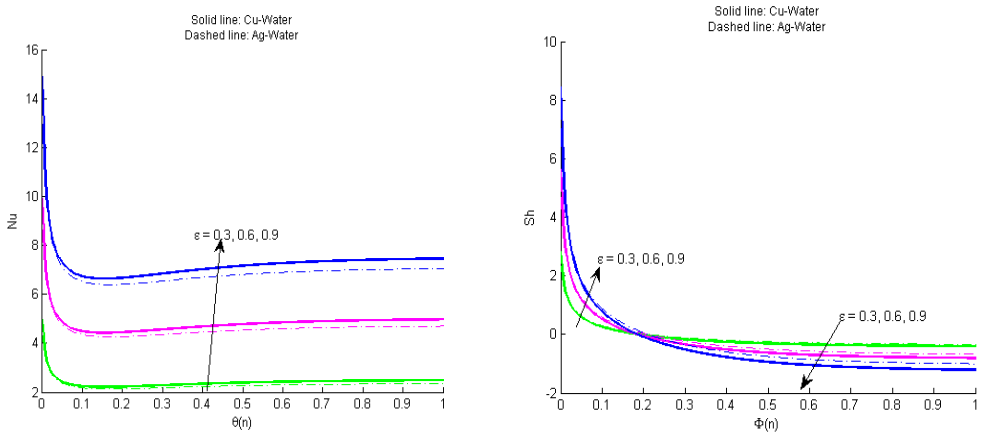

(a) (b)

Figure 6: (a) Heat transfer and (b) mass transfer coefficients when varying dimensionless time

From figure 5(b), the skin friction coefficient remains constant as dimensionless time parameter is increased. This is because when ε varied nanofluid velocity is not enhanced. This shows ε does not influence surface drag. Using figure 6(a), heat transfer coefficient increase when ε is increased. From figure 6(b) on the surface mass transfer coefficient increase with increase of dimensionless time up to critical point. This is caused by mass diffusion on the surface. Beyond this critical point, rate of mass transfer decrease with increase of dimensionless time.

5. CONCLUSION

When stretching parameter is increased, velocity of nanofluid increases and temperature of nanofluid decrease. Concentration decreases at the stretching surface up to critical point then decreases. Skin friction and heat transfer coefficients increase while mass flux decreases. At the surface nanofluid concentration increases up to critical value and beyond this point concentration decreases. When time parameter is increased velocity and skin friction coefficient remains constant, temperature, concentration, heat transfer and mass transfer coefficient increases.

Abbreviation

v_w: suction velocity

T_w: Surface temperature

C_w: Surface concentration

T_∞: Ambient temperature

C_∞: Ambient concentration

u: Fluid velocity component along x direction

v: Fluid velocity component along y

ρ_{nf}: Nanofluid density

p: Fluid pressure

ϑ_{nf}: Nanofluid kinematic viscosity

g: Unsteadiness parameter

g_a: Gravitational acceleration

B_C: Volumetric solutal expansion coefficient

σ: Electrical conductivity

B_0: Magnetic field

T: Fluid temperature

α_{nf}: Nanofluid thermal diffusivity

ρ_f: Fluid density

D_m: Concentration mass diffusivity

C_s: Concentration susceptibility

$(c_p)_{nf}$: Nanofluid specific heat capacity at constant pressure

C: Fluid concentration

Q: Volumetric rate of heat generation

k_m: mean fluid

R: Chemical reaction parameter

T_m: mean fluid.

References

[1] Ferdows M., Shakhaoath k. M., Mahmud M. A., and Afify A. A. (2017). MHD boundary layer flow and heat transfer characteristics of a nanofluid over a stretching surface sheet. *The Journal of "Sapientia" Hungarian University of Transylvania.,* 9, pp. 5-229.

[2] Ferdows, *et al* (2014). Numerical study of transient magnetohydrodynamic radiative free convection nanofluid flow from a stretching permeable surface, *Journal of Mechanical Engineering,* 228(3), 181–196.

[3] Hamad, M. A., and Pop, I. (2011). Unsteady MHD free convection flow past a vertical permeable flat plate in a rotating frame of reference with constant heat source in a nanofluid**.** *Heat and Mass TransferWärme- und Stoffübertragung © The Author(s) 2011*, 10.1007/s00231-011-0816-6.

[4] Haroun, N. A., Sibanda, P., Mondal, S., & Motsa, S. S. (2015). On unsteady MHD mixed convection in a nanofluid due to a stretching/shrinking surface with suction/injection using the spectral relaxation method. *Boundary value problems journal*, *2015*(1), 24.

[5] Hussain, A., Sarwar, L., Akbar, S., Malik, M. Y., & Ghafoor, S. (2019). Model for MHD viscoelastic nanofluid flow with prominence effects of radiation. *Heat Transfer—Asian Research*, *48*(2), 463-482.

[6] Malvandi, A., Hedayati, F. and Domairry, G. (2013). Stagnation Point Flow of a Nanofluid toward an Exponentially Stretching Sheet with Nonuniform Heat Generation/Absorption.*Journalofhermodynamics*,vol.2013,http://dx.doi.org/10.1155/2013/764827.

[7] Muhammad, T., Lu, D. C., Mahanthesh, B., Eid, M. R., Ramzan, M., & Dar, A. (2018). Significance of Darcy-Forchheimer porous medium in nanofluid through carbon nanotubes. *Communications in Theoretical Physics*, *70*(3), 361.

[8] Nor, A. (2011). Boundary layer flow past a stretching/shrinking surface beneath an external uniform shear flow with a convective surface boundary condition in a nanofluid. *Nanoscale Research Letters © Yacob et al; licensee Springer. 2011,* 10.1186/1556-276X-6-314.

[9] Puneet, R., Rama B. and Osman A. (2012). Finite element simulation of unsteady magneto-hydrodynamic transport phenomena on a stretching sheet in a rotating nanofluid. *Journal of Nanoengineering and Nanosystems,* 227(2), 77–99.